Aerodynamic Analysis of Tilt-Rotor Unmanned Aerial Vehicle with Computational Fluid Dynamics

Cheolwan Kim* and Jindeog Chung
Aerodynamics Department, Korea Aerospace Research Institute,
45 Eoeun-dong, Youseong-gu, Daejon 305-333, Korea

CFD simulation for one of tilt-rotor UAV configurations, TR-E2S1, was performed to investigate its aerodynamic characteristics. Control surfaces such as elevator and rudder were deflected and wing incidence angle was changed. Also aerodynamic stabilities were analyzed with the variation of pitch and yaw angles. The comparison of CFD with wind tunnel test results reveals the same trends in the aerodynamic characteristics and stabilities. However 12% scale wind tunnel test model is too small for accurate data collection and should build a high fidelity model for quantitative data comparison.

Key Words : Tilt-rotor, Unmanned Aerial Vehicle (UAV), CFD, Wind Tunnel Test, Drag Prediction

1. Introduction

In the early stage of flying vehicle development, it is very crucial to understand the aerodynamic characteristics of the vehicle configuration, to provide the aerodynamic database for aerodynamic performance and stability analysis and improve the configuration aerodynamically. However, vehicle analysis by wind tunnel test requires long preparation time and high cost, and Datcom prediction, based on the accumulated vehicle data, shows unrealistic result if the vehicle configuration is not conventional and the accumulated data is insufficient. Computational Fluid Dynamics (CFD) as an emerging major analysis tool does not contain any limitation to the configuration and analyze the aerodynamic characteristics within proper turn-around time and low cost. However, among development engineers, trust on the CFD results is not solid as on the wind tunnel test results and it is understood to be the big barrier for CFD being utilized broadly in developing the flying vehicle. Therefore, this paper is focused on overcoming this by presenting good correlation with wind tunnel test results.

Tilt-rotor unmanned aerial vehicle (UAV) being developed by Korea Aerospace Research Institute (KARI) is a new conceptual vehicle which is able to take-off and land vertically, and cruise at high speed. This vehicle has two highly loaded rotors tilting with nacelle from 0° to 90°. In the beginning, Bell Textron, a frontier company in the tilt-rotor aircraft development, proposed a configuration, TR-E2. However CFD analysis revealed that its aerodynamic characteristics did not satisfy the cruise condition and KARI development team began to improve the aerodynamic performance. They reviewed the performance of NACA64 series airfoils (Abbott and Doenhoff; Hoerner and Borst, 1975; Kim et al., 2004a) and finally chose NACA64621 as the airfoil of the wing. They also changed the type of tail from U-type to T-type. T-type tail is less dependent on the down wash caused by the wing at cruise flight and much less on the down wash by the high lift device of the wing at landing. T-type tail also increases the arm length of the horizontal tail

* Corresponding Author,
E-mail : cwkim@kari.re.kr
TEL : +82-42-860-2691; **FAX** : +82-42-860-2604
Aerodynamics Department, Korea Aerospace Research Institute, 45 Eoeun-dong, Youseong-gu, Daejon 305-333, Korea. (Manuscript **Received** September 12, 2005; **Revised** February 17, 2006)

Fig. 1 Smart-UAV configuration, TR-E2S1

from the moment reference center, could lead to the horizontal tail more effective and reduce the tail size. A new configuration, TR-S1 was decided by changing the wing airfoil and tail type of TR-E2. However wind tunnel test was already proceeded with the 12% scale model of TR-E2 before TR-S1 was decided, therefore, an interim configuration prototype, TR-E2S1 was created to save the model preparation time and cost by replacing the wing and tail with TR-S1 and the wind tunnel test was continued. For comparison study with wind tunnel test results, CFD simulation for TR-E2S1 was also performed (Chung et al., 2005, Kim et al., 2004b).

Therefore, in this paper, CFD analysis of TR-E2S1 was performed for different wing incidence angles and control surface deflections and rotor power effect was not considered. Figure 1 presents TR-E2S1 with nacelles, T-type tail and ventral fin. For the comparison with wind tunnel test, rotor effect and engine intake are not considered. In Section 2, general aspects of numerical analysis are explained. The simulation was conducted with a commercial CFD code, Fluent v.6.1 and the computational grid was generated with Gambit and Tgrid of Fluent package. In Section 3, the effects of the wing incidence angle, elevator and rudder were analyzed for various angles of attack, and the longitudinal and directional stabilities were investigated for yaw angle variation. In Section 4, CFD results are compared with wind tunnel test results (Chung et al., 2005).

2. Numerical Experiments

The surface grid of the 3D vehicle consists of

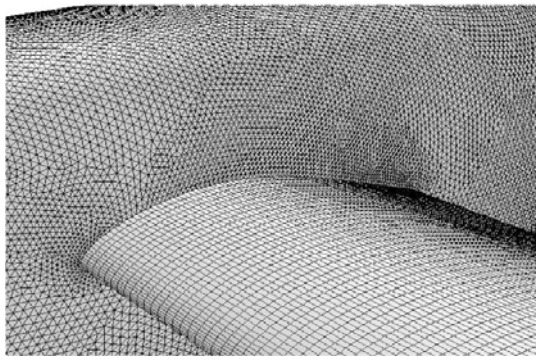

Fig. 2 Hybrid surface mesh around wing body junction

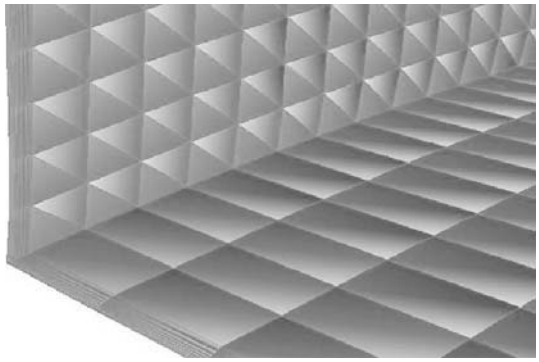

Fig. 3 Boundary layer mesh of wing body junction, generated by projection from wall, 1st layer height, $h_1=2\times10^{-4}$ m, growth rate $(h_2/h_1)=1.2$

triangle and quadrangle as shown in Fig. 2. The wing and tails are modeled with quadrangles to cluster more grid points along the main flow direction and the body surface is covered with triangles because it has several junctions. Total number of the surface grid amounts to 190,000. For accurate boundary layer computation, 10 prism layers were generated by projecting from the wall surface. Figure 3 shows the prism layers around wing body junction. The first height (h_1) of the boundary layer mesh is 1.0×10^{-4} m and the growth ratio (h_2/h_1) is 1.2. The rest of the volume is filled with tetrahedrons. Therefore total number of 3D computational grid including boundary layer mesh is about 5×10^6. The boundary conditions are applied at far-field and vehicle surface. The far-field condition is decided with free

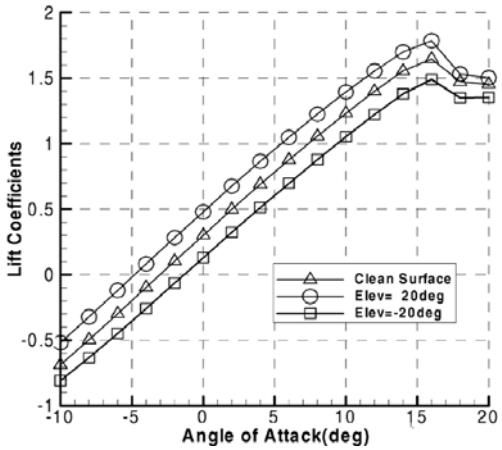

Fig. 4 Lift coefficients with control surface deflections, wing incidence angle=1°, yaw angle=0°

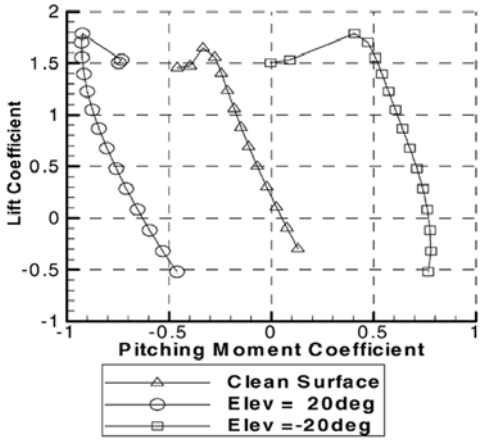

Fig. 5 Pitching moment characteristics, wing incidence angle=1°, yaw angle=0°

stream Mach number, static pressure, temperature and turbulence intensity. The whole simulation was performed at cruise condition whose speed and altitude are 400 km/h and 3 km. Therefore the Mach number, pressure and temperature at the far-field are 0.34, 70121 Pascal, 268°K and the turbulence intensity and length are 2% and 0.1 m.

After initializing the whole computational field with the far-field flow properties and iteration was carried out with 1st-order accuracy to settle down the big fluctuation of the solution. Then iteration was continued with 2nd-order scheme until the flow solution converged. Spalart-Allmaras one equation model was utilized for turbulent viscosity computation since it is known as accurate for external flow. Grid adaptation was not adopted to maintain computational condition consistent.

The validation of the numerical results was not conducted in this paper because the results were compared with different predictions generated by other analysis tools, even though they are not presented here, and accepted reasonably by the vehicle development engineers. Also the simulation results will be compared with the wind tunnel test results in Section 4.

3. Aerodynamic Characteristics with Pitch and Yaw Angle Variations

Numerical simulation was performed to investigate the stability characteristics of the vehicle by changing the pitch and yaw angles for different wing incidence, elevator and rudder deflection angles. The wing incidence angles are 1° and 4°, elevator deflection angles are ±20° and rudder deflection angle is −20°. The direction of positive elevator deflection angle is to decrease the pitching moment and make the nose down.

3.1 Effect of control surface deflection (Wing Inci. Ang.=1°, Yaw Ang.=0°)

Control surfaces, elevator and rudder, are deflected to investigate their effects on the aerodynamic characteristics of the vehicle. The wing incidence and yaw angles are 1° and 0° respectively. As the elevator deflection angle increases, lift increases linearly and 20° deflection of elevator makes 0.17 increment of lift coefficient (Fig. 4). Rudder deflection causes minor effect on the lift. Stall angle is independent of the control surface deflection and happens around angle of attack, 16°.

Figure 5 presents the pitching moment characteristics for various control surface deflections. As lift increases, pitching moment decreases. The relation between lift and pitching moment shows the longitudinal stability of the vehicle. The elevator deflection shifts the pitching moment curve to the right- or left- handed side according to the direction of the deflection angle. The positive deflection angle increases the lift of the elevator

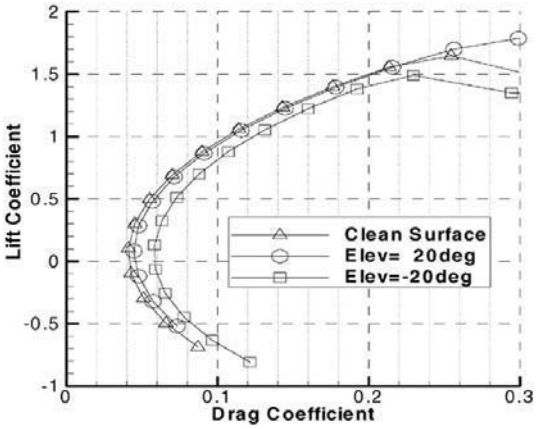

Fig. 6 Drag polar for various control surface deflections, wing incidence angle=1°, yaw angle=0°

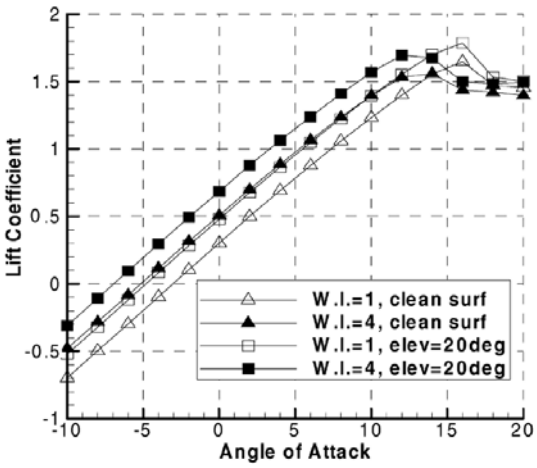

Fig. 7 Lift coefficients for wing incidence angle changes and elevator deflection (W.I. : wing incidence)

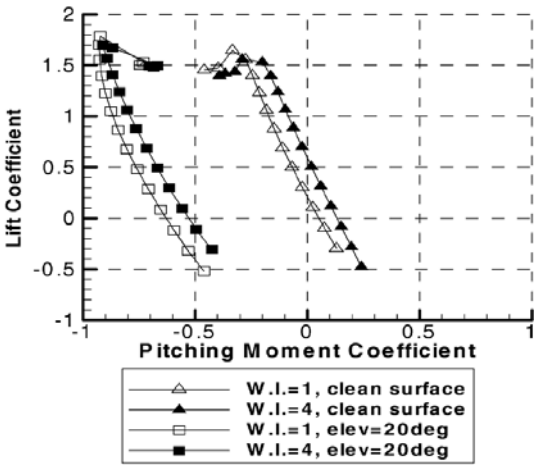

Fig. 8 Pitching moment coefficients for wing incidence changes and elevator deflection

and causes the nose of the vehicle down, and consequently shifts the pitching moment curve to the left.

Drag polar curves are shown in Fig. 6 for the elevator and rudder deflections. The minimum drag coefficient of the clean surface is 0.041 and maximum lift and drag ratio (L/D) is about 9.9 at angle of attack, 4°. Control surface deflections including elevator and rudder increase the drag and the elevator deflection in negative direction does the most.

3.2 Effect of wing incidence angle

Up to now lift, pitching moment and L/D have been analyzed for a wing incidence angle, 1°. Now, the incidence angle is increased to 4° to investigate the effect of the wing incidence angle on the aerodynamic characteristics. Figure 7 presents the lift coefficient changes for different wing incidence angles. The lift coefficient increment caused by increasing the incidence angle from 1° to 4° is about 0.2 regardless of the elevator deflection. Stall happens at angle of attack, 16° for the incidence angle, 1° and the lift curve shifts to the left-handed side as much as the increment of the incidence angle. Therefore, stall happens around 13° when the incidence angle is 4°.

Figure 8 shows the pitching moment characteristics for different wing incidence angles. As the incidence angle increases, the pitching moment increases and shifts the curve to right. This is because the aerodynamic center of the wing is not identical to that of the vehicle. If those centers are same, pitching moment of the vehicle should be constant regardless of the wing incidence angle change.

Drag polars are shown in Fig. 9 for different wing incidence angles and elevator deflection angles. Minimum drag coefficient of the clean surface (no elevator deflection) increases 0.0040 as the wing incidence angle changes from 1° to 4°. When the elevator is deflected, however,

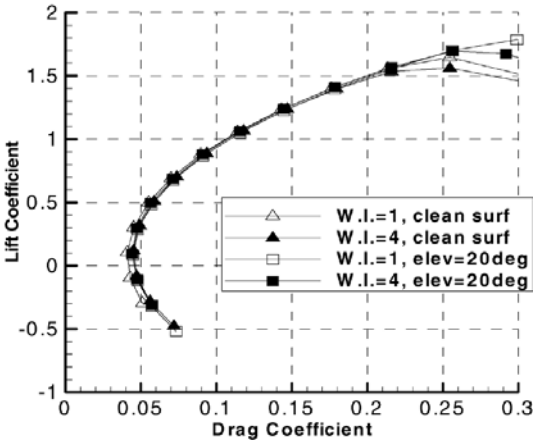

Fig. 9 Drag polars for different wing incidence and elevator deflection angles

the minimum drag is almost constant for different wing incidence angles and it is not easy to distinguish the difference.

3.3 Aerodynamic characteristics for yaw angle variation

Elevator was deflected $\pm 20°$ and rudder was deflected $-20°$ (rudder deflected to the left-handed side at the rear view) to study the directional and lateral stabilities.

Figure 10 presents side force, yawing moment and rolling moment coefficients for control surface deflections while the wing incidence angle and the pitch angle are 1°, and 0°. Elevator deflection does not change the side force and yawing moment for various yaw angles but rudder, deflected $-20°$, increases the side force and decreases the yawing moment. However, rolling moment is sensitive to the elevator deflection. As yaw angle increases, elevator deflection changes the rolling moment linearly. However rudder deflection maintains the rolling moment constant for various yaw angles.

Directional and lateral stabilities of the vehicle for different wing incidence and pitch angles are presented in Fig. 11. Different wing incidence angles generate same side force, yawing moment and similar rolling moment but higher pitch angle makes larger side force and rolling moment. As yaw angle increases, the yawing moment decreases to notice the directional stability. Positive

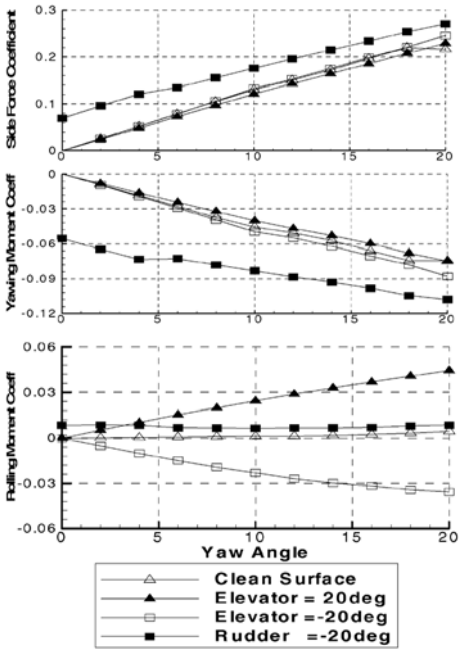

Fig. 10 Side force, yawing moment and rolling moment coefficients for control surface deflections, wing incidence angle=1°, pitch angle =0°

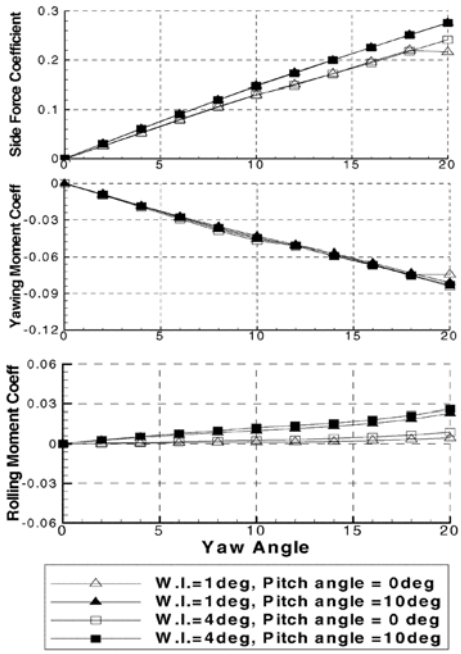

Fig. 11 Side force, yawing moment and rolling moment coefficients for different wing incidence and pitch angles

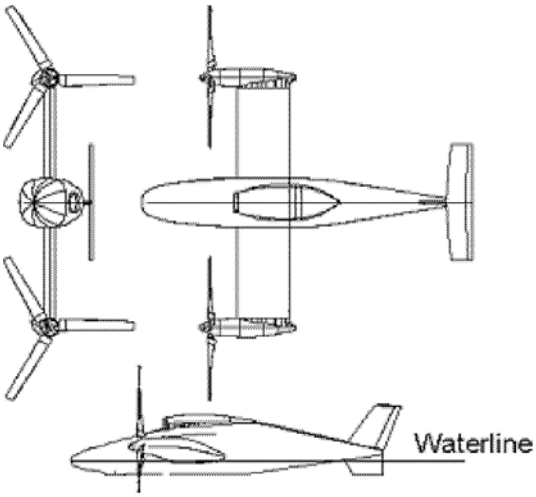

Fig. 12 General layout for TR-E2S1 configuration

yaw angle provides positive rolling moment and makes the right wing move down.

4. Comparison with Wind Tunnel Test Results

Wind tunnel test and CFD results are compared to demonstrate the correlation of two methods. The scale of the wind tunnel test model is 12% and it is assumed to be small for accurate aerodynamic data acquisition. The quantitative comparison, therefore, may be meaningless. However this model is able to present the aerodynamic characteristics and stability trends, and the comparison is focused on checking the general trends of the aerodynamic data and the stability. Results are compared for control surface deflections, wing incidence angle change and yaw angle variation.

4.1 Wind tunnel test for TR-E2S1

12% scaled model of TR-E2S1 was tested to analyze the vehicle aerodynamically.

Figure 12 shows the general layout of the vehicle configuration. The fuselage length and the wing span are 620 mm and 555 mm respectively, and the detailed dimensions are listed in Table 1. Test was performed at 1 m×0.75 m closed type wind tunnel of KARI. The real model installed on the wind tunnel is depicted in Fig. 13.

Table 1 Model geometric characteristics

Model component	Length or Area
Wing Span w/ Nacelle	555.27 mm
Wing Chord	103.1 mm
Wing Ref Area	0.0489 m^2
Horizontal Tail Area	0.0112 m^2
Horizontal Tail span	240 mm
Vertical Tail Area	0.0066 m^2
Ventral Fin Area	0.00353 m^2
Fuselage Length	620.75 mm

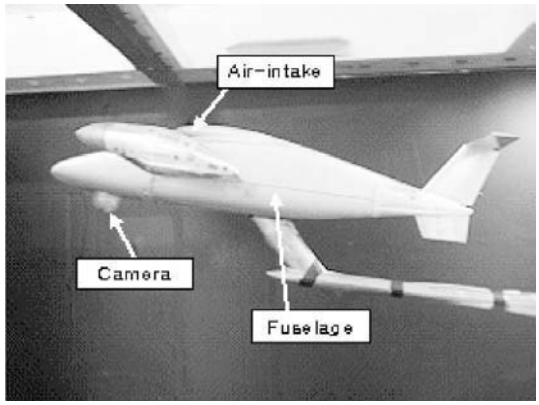

Fig. 13 12% scale TR-E2S1 model mounted on sting balance of 1 m×0.75 m wind tunnel

4.2 Control surface deflection (wing incidence angle=0°, yaw angle=0°)

When the wing incidence angle and yaw angle are 1° and 0° respectively, Fig. 14 compares lift curves of wind tunnel test and numerical simulation. For an angle of attack, 0°, lift coefficients of test result and CFD are 0.2 and 0.3 and elevator deflections of test model and CFD make lift coefficient increments of 0.1 and 0.17. Stall angle predicted by CFD analysis is about 16° but the angle by wind tunnel test is more than 20°. CFD analysis predicts higher lift than wind tunnel test and makes bigger lift changes for elevator deflection.

Figure 15 compares pitching moment coefficients of both methods. CFD analysis predicts higher pitching moment increments than wind tunnel test. Elevator deflection (deflection angle =20°) of CFD model decreases pitching moment

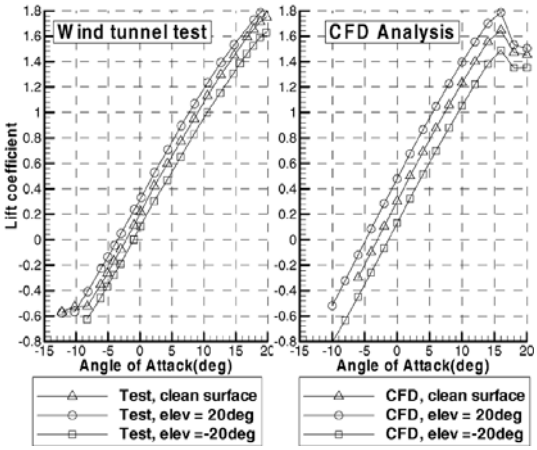

Fig. 14 Lift coefficients comparison, wing incidence angle=0°, yaw angle=0°

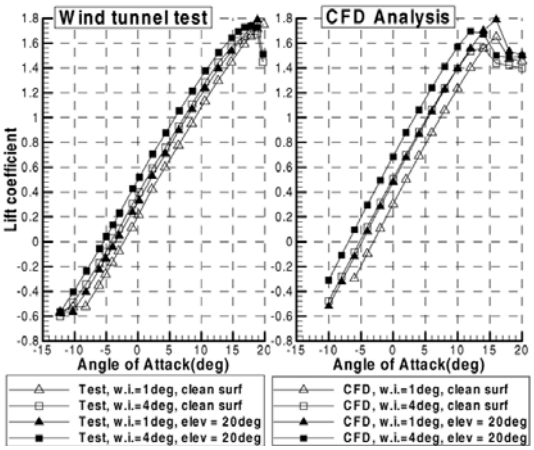

Fig. 16 Comparison of lift coefficients for wing incidence angle changes

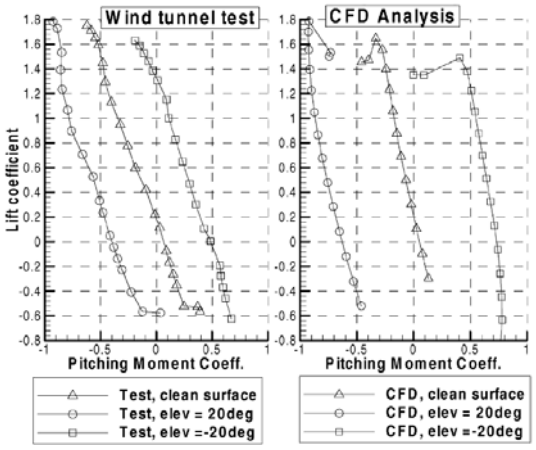

Fig. 15 Comparison of pitching moment coefficients, wing incidence angle=0°, yaw angle=0°

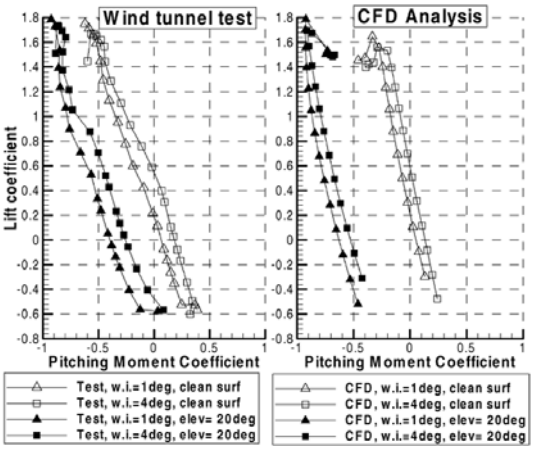

Fig. 17 Comparison of pitching moment characteristics for wing incidence angles

coefficient ($\triangle C_M = -0.67$) and the deflection of wind tunnel test model decreases pitching moment less than CFD model ($\triangle C_M = -0.45$).

4.3 Wing incidence angle effect

As presented in Fig. 16, wing incidence angle change of both models increase lift coefficients almost same amount ($\triangle C_L = 0.2$). Furthermore both methods predict the same maximum lift. However, the stall angle predicted by CFD is less than that of wind tunnel test. For wing incidence angle, 4°, stall angle of CFD is about 13° and wind tunnel test predicts about 18°.

Figure 17 demonstrates the pitching moment characteristics for wing incidence angle change. Both methods predict the longitudinal stability that higher angle of attack generates less pitching moment and make the nose of the vehicle down. However wind tunnel test results (Fig. 17 left) show larger pitching moment increment than CFD.

4.4 Yaw angle variation

Figure 18 compares the side force, yawing moment and rolling moment coefficients for wing incidence angle, 1° and pitch angle, 0°. The trends for side force, yawing moment and rolling moments generated by both methods are very similar.

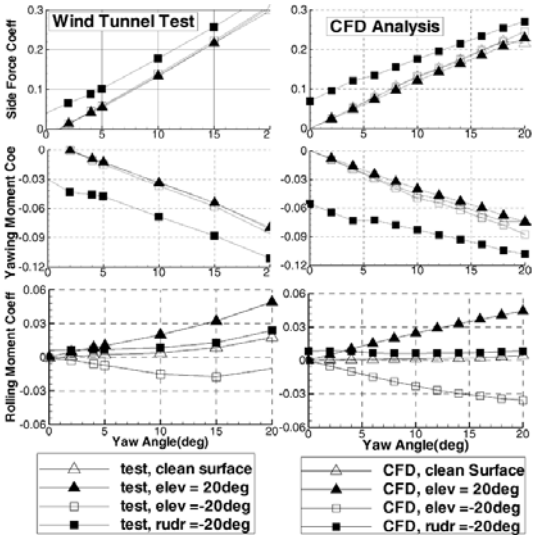

Fig. 18 Comparison of side force, yawing moment and rolling moment coefficients for control surface deflections, wing incidence angle= 1°, pitch angle=0°

However the side force of the wind tunnel test is not symmetric and has negative value at yaw angle, 0°. The wind tunnel test generates more side force than CFD for any control surface deflection but the test predicts very similar yawing moment to CFD. At the elevator deflection, −20°, the rolling moment of the test increases for yaw angle beyond 15° meanwhile the rolling moment of CFD decreases.

5. Conclusions

One of the models for tilt-rotor UAV development, TR-E2S1, was tested numerically to understand the vehicle aerodynamically. Hybrid meshes were generated to present the vehicle surface and flow region. Numerical experiment was conducted by deflecting the control surfaces, elevator and rudder. According to the numerical result, the minimum drag coefficient is 0.041 and maximum lift and drag ratio is about 9.9 at angle of attack, 4° and wing incidence angle, 1°. The vehicle also shows the lateral stability and makes the nose down at increasing angle of attack. Elevator deflection (angle=20°) makes 0.17 increment of the lift coefficient but does not change the stall angle.

The comparison of CFD result with wind tunnel test result reveals same trends of the aerodynamic characteristics and stabilities. However 12% scale wind tunnel test model is too small for accurate data collection and should be enlarged for quantitative data comparison.

Acknowledgments

This works was supported by Smart UAV development Program, one of the 21st Century Frontier R&D Programs funded by the Ministry of Commerce, Industry, and Energy of Korea.

References

Abbott, I. and Doenhoff, A., Theory of Wing Sections, Dover Publications.

Chung, J., Yoon, S. and Cho, T., 2005, "Wind Tunnel Test of Smart Un-manned Aerial Vehicle (SUAV) for TR-E2S1 Configuration," *KSME B*, Vol. 29 No. 3 pp. 295～305

Hoerner, S. F. and Borst, H. V., 1975, Fluid-Dynamic Lift, Published by Hoerner, L.A.

Kim, C., Chung, J. and Lee, J., 2004a, "CFD Analysis of Tilt-Rotor Unmanned Aerial Vehicle," *3rd National Congress on Fluids Engineering*, Aug. 26-28, Jeju, Korea

Kim, C., Chung, J. and Lee, J., 2004b, "Aerodynamic Analysis of Smart UAV with CFD," Proceeding of Korean Society of Computational Fluids Engineering